NASA/TM-20230007568

Recrystallization of a Shot Peened Single Crystal Nickel-Base Superalloy

Timothy P. Gabb, Christopher A. Kantzos, Timothy M. Smith, Jack Telesman, and Laura J. Evans
Glenn Research Center, Cleveland, Ohio

Ralph J. Pawlik
HX5, LLC, Brook Park, Ohio

October 2023

NASA STI Program . . . in Profile

Since its founding, NASA has been dedicated to the advancement of aeronautics and space science. The NASA Scientific and Technical Information (STI) Program plays a key part in helping NASA maintain this important role.

The NASA STI Program operates under the auspices of the Agency Chief Information Officer. It collects, organizes, provides for archiving, and disseminates NASA's STI. The NASA STI Program provides access to the NASA Technical Report Server—Registered (NTRS Reg) and NASA Technical Report Server—Public (NTRS) thus providing one of the largest collections of aeronautical and space science STI in the world. Results are published in both non-NASA channels and by NASA in the NASA STI Report Series, which includes the following report types:

- TECHNICAL PUBLICATION. Reports of completed research or a major significant phase of research that present the results of NASA programs and include extensive data or theoretical analysis. Includes compilations of significant scientific and technical data and information deemed to be of continuing reference value. NASA counter-part of peer-reviewed formal professional papers, but has less stringent limitations on manuscript length and extent of graphic presentations.

- TECHNICAL MEMORANDUM. Scientific and technical findings that are preliminary or of specialized interest, e.g., "quick-release" reports, working papers, and bibliographies that contain minimal annotation. Does not contain extensive analysis.

- CONTRACTOR REPORT. Scientific and technical findings by NASA-sponsored contractors and grantees.

- CONFERENCE PUBLICATION. Collected papers from scientific and technical conferences, symposia, seminars, or other meetings sponsored or co-sponsored by NASA.

- SPECIAL PUBLICATION. Scientific, technical, or historical information from NASA programs, projects, and missions, often concerned with subjects having substantial public interest.

- TECHNICAL TRANSLATION. English-language translations of foreign scientific and technical material pertinent to NASA's mission.

For more information about the NASA STI program, see the following:

- Access the NASA STI program home page at http://www.sti.nasa.gov

- E-mail your question to help@sti.nasa.gov

- Fax your question to the NASA STI Information Desk at 757-864-6500

- Telephone the NASA STI Information Desk at 757-864-9658

- Write to:
  NASA STI Program
  Mail Stop 148
  NASA Langley Research Center
  Hampton, VA 23681-2199

NASA/TM-20230007568

Recrystallization of a Shot Peened Single Crystal Nickel-Base Superalloy

Timothy P. Gabb, Christopher A. Kantzos, Timothy M. Smith, Jack Telesman, and Laura J. Evans
Glenn Research Center, Cleveland, Ohio

Ralph J. Pawlik
HX5, LLC, Brook Park, Ohio

National Aeronautics and
Space Administration

Glenn Research Center
Cleveland, Ohio 44135

October 2023

Acknowledgments

The authors acknowledge the support of NASA's Aeronautics Research Mission Directorate (ARMD) Advanced Air Transport Technology (AATT) Project Office and the Transformational Tools and Technologies Program.
The authors thank Dr. Laura Wilson for her thoughtful review of this manuscript.

This work was sponsored by the Advanced Air Vehicle Program
at the NASA Glenn Research Center

Level of Review: This material has been technically reviewed by technical management.

This report is available in electronic form at https://www.sti.nasa.gov/ and https://ntrs.nasa.gov/

Recrystallization of a Shot Peened Single Crystal Nickel-Base Superalloy

Timothy P. Gabb, Christopher A. Kantzos, Timothy M. Smith, Jack Telesman, and Laura J. Evans
National Aeronautics and Space Administration
Glenn Research Center
Cleveland, Ohio 44135

Ralph J. Pawlik
HX5, LLC
Brook Park, Ohio 44142

Summary

Single crystal nickel-base superalloys used as turbine engine blades can have much higher creep and fatigue resistance than many polycrystalline superalloys. This is due to their advantage of removed weak grain boundaries, as well as lower elastic modulus in the [001] single crystal orientation, the primary loading direction. However, significant plastic deformation during machining can encourage new grains to form (i.e., recrystallization) at damaged surfaces during subsequent solution heat treatment or during service at sufficiently high temperatures. This can degrade the advantages described. Single crystal superalloys intended for other high-temperature applications, such as structural assemblies including turbine disk rim segments, could have many exposed surfaces in a variety of surface conditions resulting from component preparations, including low-stress grinding followed by shot peening, which could further encourage subsequent recrystallization. This study assessed the relationship between the effects of such surface conditioning and thermal exposure on subsequent recrystallization tendencies.

Nomenclature

AMS2430	Aerospace Material Specifications standard for shot peening
AMS2432	Aerospace Material Specifications standard for shot peening, computer monitored
CCW14	conditioned cut wire shot
EBSD	electron back scatter diffraction
IPF	inverse pole figure
IQ	image quality
LAB	low angle boundaries

Introduction

Single crystal nickel-base superalloys used as turbine engine airfoils can have much higher creep and thermal fatigue resistance required for blades and vanes than polycrystalline superalloys due to the absence of weak grain boundaries, as well as the low elastic modulus in the [001] single crystal growth direction (Refs. 1 and 2). This has allowed an increase in the turbine rim inlet temperatures for improved performance and efficiency. However, these advantages in performance require constraints on acceptable levels of single crystal defects, such as macroscopic grain boundaries at low angles to the primary grain (i.e., low angle boundaries or LAB), higher angle boundaries, small new grains nucleated at the blade surface (a.k.a. freckles), larger new grains, and also the single crystal blades' orientation, typically

degrees off of the [001] direction and the orientation of a transverse [010] direction with respect to blade geometry. Therefore, single crystal turbine airfoils, which are frequently used with as-cast surfaces, are grain etched and inspected before and after heat treatments to ensure these aspects conform to acceptability limits (Ref. 3).

Studies have shown, even in early adaptations of single crystal superalloys as airfoils (Refs. 4 and 5), that these single crystal defects can occur after casting, during heat treatment, or during service, at locations that have experienced significant plastic deformation. A systematic study (Ref. 6) of several single crystal superalloys (CMSX-6, CMSX-11B, PWA 1483, and SRR 99) indicated low-temperature plastic deformation as small as 1 percent is sufficient to encourage subsequent recrystallization at exposed surfaces. Varied annealing heat treatments were not successful in removing enough of this plastic deformation to avoid recrystallization. Surface oxidation was not necessary for recrystallization, which also occurred in vacuum.

These aspects were extensively investigated for CMSX-4, a highly successful, commercially available, single crystal nickel-base superalloy. It is used in a variety of aerospace gas turbine engines as turbine blades and vanes (Ref. 3). Several studies (Refs. 7, 8, and 9) of this recrystallization problem have focused on this alloy. In one illuminating study (Ref. 7), indentations at room temperature followed by tensile tests at varied temperatures were used to produce plastic strain; then, annealing experiments were performed to study recrystallization tendencies and kinetics. Plastic strains exceeding 1 percent were sufficient to encourage recrystallization in subsequent extended heating to temperatures exceeding 1,200 °C (2,192 °F). Plastic strains introduced at high temperatures were more effective at encouraging this subsequent recrystallization. In a subsequent focused study (Ref. 8), the effects of indentations on plastic strains at room temperature and subsequent recrystallization tendencies were further studied and modeled. For spherical indentations introduced at room temperature onto single crystal surfaces nearly normal to the [001] crystallographic direction, plastic strains were predicted to extend further in the <011> directions, consistent with the greater extent of subsequent recrystallization in those directions. However, the effects of other machining and handling processes at room temperature on plasticity and subsequent recrystallization tendencies were not considered. A later detailed series of experiments and modeling of plastic strains, introduced at high temperatures during casting of CMSX-4 (Ref. 9), indicated inelastic strains introduced at stress concentrations from the mold during initial cooling can be severe, encouraging subsequent recrystallization. This work also showed in more detail how tensile plastic deformation at temperatures higher than 1,200 °C (2,192 °F) was more effective in promoting recrystallization.

These studies all showed that excursions to very high temperatures were needed for new grains to recrystallize and grow for the evaluated levels of plastic deformation. This has been associated with the need for sufficiently high temperatures to dissolve most or all of the gamma prime precipitates, which can hinder grain boundaries from advancing during grain growth. One corresponding approach to minimize this risk is to limit the temperatures experienced during heat treatment and service. For example, the first heat treatment step of fully homogenizing the alloy and dissolving all gamma prime precipitates, requiring a slow ramp up to a temperature near 1,310 °C (2,390 °F) for CMSX-4, could be reduced or even omitted (Ref. 10). This could leave some coarse gamma prime precipitates undissolved, not refined by nucleation, growth, and coarsening during a controlled quench from the solution heat treatment followed by the aging heat treatments. In turn, this can lower creep resistance to some degree, but it could avoid recrystallization events. In the most conservative case, as-cast material can be given only the two steps of the double aging heat treatment—a primary aging step of 1,150 °C (2,102 °F) for 4 h and a secondary aging step of 871 °C (1,600 °F) for 20 h—to dissolve, reprecipitate, and refine a percentage of the gamma prime. For some applications where the low modulus of single crystals can be used to sufficiently reduce principal stresses, the single crystal may even have acceptable mechanical response in

the as-cast form. This latter case would then only need to be limited in service temperatures to prevent recrystallization.

The single crystal superalloy (Ref. 11) tested in the present study has a composition similar to that of CMSX-4 (Table I). This alloy could have a higher gamma prime solvus than CMSX-4. The overall effect of this higher gamma prime solvus on recrystallization tendencies at high temperatures is not clear. Higher required solution heat treatment temperatures could increase the risk for recrystallization with a given surface condition. However, a fixed high application temperature could leave more gamma prime undissolved in this present alloy than in CMSX-4, potentially reducing the risk of recrystallization.

Other applications of single crystal superalloys in turbine engine rotating hardware could also benefit engine efficiency and performance. For example, work has been done to braze cast single crystal superalloy rim segments onto powder metal disk superalloy webs (Ref. 12). Such a rim could have higher creep, tensile, and dwell fatigue resistance than conventional disk superalloys and allow significantly increased rim temperatures (Ref. 13). This would require joining single crystal rim segments to a superalloy disk bore-web section, potentially with prejoining and postjoining heat treatments. Prejoining and postjoining machining processes on these rim sections could be necessary to prepare the surface to be joined, then to incorporate necessary features such as cooling holes, bolt holes, fillets, blade slots, and other details. Candidate machining processes could include drilling, turning, low-stress grinding, and others. Surface conditioning is often subsequently used to produce uniform surface finish and compressive residual stresses on machined disk surfaces to suppress life-limiting fatigue cracking there. This is most often accomplished by shot peening. During service, these single crystal disk rim segments could be locally compressed at turbine blade slot contact points and impacted at very high speed by foreign object intrusions. These service issues could enable recrystallization. The effects of such candidate surface machining and surface conditioning processes, as well as service conditions, on the potential for recrystallization would need to be screened early on for such applications. Rotating components need sufficient fatigue life, and recrystallized grains of crystallographic orientation diverging from [001] could promote premature initiation of fatigue cracks.

The objective of this study was to screen the effects of shot peening onto low-stress ground surfaces on subsequent recrystallization tendencies in a single crystal superalloy. Specimens were prepared with varied shot peening conditions, then given varied exposures. The effects of these conditions on surface roughness and depth of recrystallization were evaluated.

Material and Procedure

The comparison in Table I shows that the single crystal superalloy test material had a composition in weight percent very similar to that typically reported for CMSX-4 (Ref. 3), which was cited in many of the previously referenced studies of recrystallization. A bar of the alloy obtained for this study was approximately 26 mm in diameter and 200 mm in length; it had been cast, hot isostatically pressed, solution heat treated, and aging heat treated using typical industry practices as described in Reference 11. Three specimen cubes 18 mm per side were prepared by electrical discharge machining, with all faces subsequently low-stress ground.

Two opposing faces of each cube were shot peened. The shot peening procedures, including intensity and coverage calibrations, nozzle design, specimen masking, and other quality control issues, were performed according to AMS2432 specifications by Metal Improvement Company, Curtiss-Wright Surface Technologies, Blue Ash, Ohio. Conditioned cut stainless steel wire with a roughly spherical mean diameter of 360 μm (0.014 in.) after conditioning (CCW14) was used. Shot peening at the lowest intensity of 4 N was performed in accordance with AMS2430 specifications in order to calibrate intensity accurately at this least aggressive condition. Specimens were held in a fixture while a translating nozzle

maintained at a constant angle applied the shot at constant pressure and flow rate, using a computer-controlled automated system. As listed in Table II, shot peening intensities were varied from 4 N to 8 A (~24 N), with coverages of 100 to 800 percent. The 100 percent coverage was defined as the time necessary to indent all of the exposed surface; 800 percent coverage was 8 times that length of time. Centered shot peening conditions of 14 N intensity and intermediate coverages were also included. For clarity in comparing the effects of varied intensity, the highest intensity of 8 A is referred to here as "24 N" to allow the use of a consistent unit in the discussion and for the variable of intensity *I* in the regressions. Reports of shot peening single crystal superalloys using these varied conditions, which are more typically applied for disk superalloys, could not be found in the literature. To provide a reasonable baseline for comparison, low-stress ground witness specimens of the same configuration and approximate dimensions were prepared from LSHR, a powder metallurgy disk superalloy (Ref. 13). These witness specimens were shot peened in the same fixture, machine, and facility using the same conditions as for the present single crystal superalloy.

The shot peened surfaces were examined prior to exposures using a JSM-6100 scanning electron microscope (JEOL USA). Surface roughness was measured using white light interferometry with a NewView™ 7200 optical profiler (Zygo Corporation). For high-temperature exposures of shot peened single crystal superalloy, specimens were placed inside an alumina boat, which was then overwrapped with two layers of tantalum (Ta) foil. They were exposed in a vacuum of 10^{-6} torr at temperatures of 1,200 and 1,300 °C (2,192 and 2,372 °F), for times of 1 and 10 h.

Electron back scatter diffraction (EBSD) imaging was completed on a Zeiss Augira Electron Microscope, using an EDAX Hikari EBSD detector. The data were processed using TSL OIM Analysis software, version 7 (EDAX, Inc.). This revealed that the shot peening caused heavy deformation and large orientation variations near the surface, requiring the data to be cleaned up. First, an iterative grain dilation algorithm (max. misorientation 5°, min. grain area of 10 μm^2) was used to assign grains to ambiguous areas. Next, the image quality (IQ) metric was used to filter out the background using a two standard deviations threshold. Figure 1(a) is the raw EBSD inverse pole figure (IPF) map, showing the ambiguous areas near the surface and the background to the left of the surface. Figure 1(b) is the IQ map, in which areas of poor signal are dark. Figure 1(c) shows the overlaid IPF and IQ maps. Figure 1(d) is a processed grain map created with a custom MATLAB script used to prepare the maps for automated measurement of the recrystallization depth. Note that Figure 1(d) does not depict orientations; instead, each color represents a unique grain where blue/green grains are recrystallized grains, and the red grain is the single crystal. The MATLAB script allowed for automated measurement of the recrystallization depth at 15 evenly spaced locations along the image. Figure 2 illustrates these depth measurements in black. Furthermore, along each of the 15 measurement lines, the mean linear intercept grain widths were measured for recrystallized grains. Note that the data processing steps were intended to reduce noise, so smaller grains may not be represented accurately in these measurements.

Statistical evaluations of responses were performed using JMP® statistical analysis software, version 17 (JMP Statistical Discovery LLC) (Ref. 14). These linear regressions were intended to objectively screen for significant variables and linear relationships. Variables *V* were expressed in standardized form *V′* using Equation (1):

$$V' = \frac{V - V_{\text{mid}}}{0.5 * (V_{\text{max}} - V_{\text{min}})} \tag{1}$$

In Equation (1), for each independent variable, *V* is the actual value measured, V_{max} is the maximum value measured across all cases, V_{min} is the minimum value measured across all cases, and $V_{\text{mid}} = (V_{\text{max}} + V_{\text{min}})/2$.

This generates a range of values from –1 to +1 for each of the independent variables evaluated. Regression model equations were derived by comparing the results of both forward and reverse stepwise selection of terms, with a 90 percent probability of significance required for inclusion of a term. The coefficient of determination adjusted for the number of predictive variables (R^2_{adj}) and the root of the mean of summed squares of remaining errors between the estimated and actual responses (rms error) were used as indications of goodness of fit. These expressions using standardized variables V' are useful when comparing effects in relationships, as the relative effect of each variable and variable interaction among shot peening intensity I', shot peening coverage C', exposure temperature T', and exposure time t' on the response can be assessed in the derived regression equation by directly comparing the magnitude of the coefficient for each term (Ref. 14).

Results

Roughness

The varied shot peening conditions significantly influenced surface roughness. Typical images of the shot peened surfaces are shown in Figure 3 and Figure 4. The dimples induced by impacting shot clearly increase in size with increasing intensity for both the single crystal and LSHR witness specimens. The edges of these dimples correspondingly become more prominent with increased intensity. The average roughness R_a, root mean square roughness R_{ms}, and peak-valley roughness R_z of the specimens are tabulated in Table III. Surface roughness changed in a very similar manner for the varied conditions in the single crystal and LSHR, as shown in Figure 5. This indicated that the surface of the single crystal superalloy responded in a manner comparable to conventional polycrystalline superalloys such as LSHR, and that these shot peening conditions were reasonable. All three measures of roughness significantly increased with increasing intensity *I*, as shown in the plots versus intensity in Figure 6(a) and (b). The effects of coverage *C* are not as easily discernable in Figure 6(c) and (d), as the extreme values of coverage were evaluated at both high and low intensities. Consequently, linear regression of roughness versus coverage did not indicate a significant correlation existed. Multiple linear regression allowed successful evaluation of both intensity and coverage, as well as their interaction. The resulting relationships to estimate each measure of roughness of the single crystal in microns are listed in Equations (2) to (4), along with the coefficients of determination and rms errors:

$$R_a = 1.401 + 0.780 * I' - 0.150\ C' - 0.130 * I' * C' \qquad R^2_{adj} = 0.992, \text{ rms error} = 0.063\ \mu m \tag{2}$$

$$R_{ms} = 1.766 + 0.975 * I' - 0.195\ C' - 0.175 * I' * C' \qquad R^2_{adj} = 0.988, \text{ rms error} = 0.099\ \mu m \tag{3}$$

$$R_z = 9.756 + 5.075 * I' - 1.212\ C' - 0.970 * I' * C' \qquad R^2_{adj} = 0.983, \text{ rms error} = 0.613\ \mu m \tag{4}$$

The roughness relationships each had a high adjusted coefficient of determination and a low rms error, indicating satisfactory results. These equations indicate that all three measures of roughness increased most strongly with increasing intensity and less strongly with decreasing coverage. Combinations of high intensity and low coverage gave enhanced roughness. The comparisons of measured roughness versus the roughness estimated using the relationships described using Equation (2) to (4) shown in Figure 7(a) indicate the relationships were suitable. The cube plot in Figure 7(b) indicates how markedly the estimated mean values of peak-valley roughness R_z change with increasing intensity and decreasing coverage.

Recrystallization Responses

Specimen surfaces that were low-stress ground but not shot peened did not display notable formation of recrystallized gains after these high-temperature exposures. Consequently, these surfaces are not discussed further.

The degrees of recrystallization experienced for shot peened surfaces varied greatly with shot peening conditions and exposure conditions of temperature and time. Images from EBSD evaluations of each specimen given varied shot peening and exposures are presented in Figure 8 to Figure 10. Depths of recrystallization varied from 0 to nearly 200 μm. However, it is also apparent that recrystallized grains did not always form a continuous layer along the surface. Especially for surfaces shot peened at an intensity of 4 N, the recrystallized grains were not always numerous enough to form a continuous layer at the surface of consistent depth. Therefore, two measures of depth were generated for comparisons. Mean depth was measured by overlaying evenly spaced lines oriented perpendicular to the surface. An alternative measure of depth was generated with a line placed parallel to the surface, adjusted so that 50 percent of the line crossed recrystallized grains. The latter measurement will be referred to as the 50 percent recrystallized depth. These measurements are tabulated in Table IV.

Direct relationships between these measures of depth and any one of the four variables were not noteworthy. Mean and 50 percent recrystallized depths are shown as functions of intensity, coverage, exposure temperature, and exposure time in Figure 11. Inspection of Table IV and the plots in Figure 11 indicate the two measures of depth had quite comparable values for the varied conditions. As indicated in Figure 11, linear regression of the mean depth with each variable produced very low coefficients of determination R^2, which could not be considered significant. However, the average depth of recrystallization was found to increase with increasing intensity, temperature, and time.

Stepwise selection with multiple linear regressions allowed successful evaluation of varied intensity, coverage, temperature, and time, as well as all of their interactions. The resulting relationship to estimate each measure of depth in microns is listed in Equations (5) and (6), along with the adjusted coefficient of determination and rms error.

$$\begin{aligned} \text{50\% recrystallized depth} = {} & 39.458 + 30.219 * I' + 20.592 * T' + 19.925 * t' + 22.756 * I' * T' \\ & + 16.656 * I' * t' + 17.325 * T' * t' \\ & R^2_{adj} = 0.769, \text{ rms error} = 25.637\ \mu\text{m} \end{aligned} \tag{5}$$

$$\begin{aligned} \text{Mean depth} = {} & 41.241 + 30.201 * I' + 21.913 * T' + 18.753 * t' + 22.866 * I' * T' \\ & + 17.419 * I' * t' + 15.541 * T' * t' \\ & R^2_{adj} = 0.771, \text{ rms error} = 25.360\ \mu\text{m} \end{aligned} \tag{6}$$

The derived relationships for depth of recrystallization each had very similar constants, satisfactory adjusted coefficients of determination, and low rms error, indicating consistent and useful results for inspecting trends. These equations indicate that both measures for depth of recrystallization increased most strongly with increasing shot peening intensity and less strongly with increasing temperature and time of exposure. Among interactions, the combination of high intensity with high exposure temperature gave the strongest enhancement in depth of recrystallization. Combinations of high intensity with high exposure time and high exposure temperature with high exposure time gave weaker enhancement in depth of recrystallization. Comparisons of measured versus estimated depths of recrystallization are shown in Figure 12(a), indicating comparable results for the two measures of depth. The cube plot of Figure 12(b)

indicates how much estimated mean values of mean recrystallized depth change with increasing shot peening intensity, exposure temperature, and exposure time.

The sizes of recrystallized grains also varied substantially with shot peening conditions and exposure conditions of temperature and time. This is evident in the images from EBSD evaluations presented for all conditions in Figure 8 to Figure 10. The number of recrystallized grains detected was sometimes limited among the varied conditions, but the grains analyzed tended to have crystallographic orientations far removed from the underlying single crystal. Sufficient numbers of grains to enable comparisons of the degree of randomness in orientation for varied conditions would take further analyses of specimens treated to give greater numbers of grains. However, the existing images suggested random crystallographic orientations were prevalent for the recrystallized grains. Growth of these grains during exposures appeared to be enhanced for higher shot peening intensities and higher exposure temperatures. Grains appeared to become fairly equiaxed in all directions with increasing time at 1,200 °C (2,192 °F). However, many grains preferentially grew parallel to the surface with increasing time of exposure at 1,300 °C (2,372 °F).

The mean values for measurements of grains using linear intercept distance perpendicular to the surface are included in Table IV, and are displayed as functions of intensity, coverage, exposure temperature, and exposure time in Figure 13. Direct relationships between this mean grain size and any one of the four variables were not significant, as indicated by the very low coefficient of determination (R^2) generated for each derived linear regression equation. Stepwise selection with multiple linear regression allowed evaluation of mean grain size with varied intensity, coverage, temperature, and time, as well as all of their interactions. The resulting relationship to estimate mean grain size in microns is listed in Equation (7), along with the adjusted coefficient of determination and rms error:

$$\begin{aligned} \text{Mean grain size} = {} & 14.183 + 8.761 * I' + 7.568 * T' + 8.15 * t' + 7.273 * I' * T' \\ & + 6.133 * I' * t' + 6.795 * T' * t' \\ R^2_{adj} = {} & 0.684, \text{ rms error} = 11.01\ \mu\text{m} \end{aligned} \tag{7}$$

The derived relationship provided a lower adjusted coefficient of determination than those for the depths of recrystallization but also a lower rms error, so it was still judged useful for inspecting trends. The relationship indicates that this measure of grain size increased most strongly for exposed specimens with increasing shot peening intensity and then with increasing time and temperature of exposure. Among interactions, the combination of high intensity with high exposure temperature gave the strongest enhancement in recrystallized grain size. Combinations of high exposure temperature with high exposure time and high shot peening intensity with high exposure time gave weaker enhancements in grain size. Satisfactory comparisons of measured versus estimated mean grain size are indicated in Figure 14(a). The cube plot of Figure 14(b) illustrates how much estimated mean values of grain size increase with increasing shot peening intensity, exposure temperature, and exposure time.

Discussion

Shot peening is usually applied to superalloys for providing a uniform surface finish and beneficial compressive residual stresses near the surface. The shot peening conditions applied here have been very commonly employed on polycrystalline nickel-base superalloys used in gas turbine engines, but they have not been reported for single crystal superalloys. Given that the roughness values measured here were very similar to those measured on polycrystalline powder metallurgy disk superalloy LSHR for the same shot peening procedures and conditions, the selected conditions do appear reasonable and give predictable roughness results. Residual stresses, as conventionally measured by x-ray diffraction on polycrystalline

superalloys, could not be determined on the tested single crystal superalloy surfaces at this time. Measurements on the LSHR witness specimens indicated satisfactory compressive residual stresses from 1,000 to 1,320 MPa (145.0 to 191.4 ksi) were generated by these shot peening conditions near the surface. However, the high application temperatures requiring single crystal superalloys would be expected to relax a majority of the residual stresses (Ref. 15), so these stresses were not considered further for this study.

To minimize tendencies for recrystallization, analyses of the results indicate lowest intensity and lowest coverage were required. When combined with minimized exposure temperature and time, material treated in this condition displayed no recrystallization. This shot peening condition also gave low, though not the lowest, roughness. However, the surface area of these specimens was evaluated on a small cross section over a width of only 18 mm. Therefore, it could be useful to screen for this response at the current conditions and even lower shot peening intensities over much greater distances and multiple trials. Others have also found that shot peening can promote recrystallization in subsequent exposures at high temperatures, to the detriment of fatigue life (Ref. 16). Therefore, in relevant applications, fatigue could be necessary as a screening tool. Rather than conventional shot peening, processes such as ultrasonic shot peening (Ref. 17) or laser shot peening (Ref. 18) could also be considered for screening.

Alternatively, it might also be useful in some applications to strive for a surface layer of controlled and uniform depth made up of recrystallized fine, randomly oriented grains, which could provide isotropic, compliant properties there. This did appear to be possible here within the ranges of the test conditions. For example, estimation using the resulting Equation (6) and (7) indicate shot peening at a mid-level intensity of 14 N, followed by exposure at a mid-level temperature of 1,250 °C for a mid-level time of 5.5 h could produce a mean recrystallized depth of 41.2 μm and a mean grain size of 14.2 μm. Joint optimization of these two equations to maximize recrystallized depth while minimizing mean grain size indicated shot peening at a higher intensity of 19.7 N, followed by exposure of 1,300 °C for 1 h would give a larger mean recrystallized depth of 49.1 μm, with a finer estimated mean grain size of 12.4 μm. These two sets of conditions could help establish the bounds for more refined screening to attain high and consistent depth of recrystallization to fine, randomly oriented grains. Such additional screening could be necessary, as these relatively high shot peening intensities and temperatures could produce a stronger driving force for recrystallization than that present at the lower levels of the present screening study, resulting in potentially nonlinear responses.

In these respective cases, the random occurrence of an unwanted recrystallized grain or variability of depth and grain size of an intended layer of grains would need to be evaluated over greater surface lengths and numbers of specimens. Screening of such conditions could take into consideration the prospective applications, as mechanical properties such as fatigue resistance could be influenced by recrystallization response, as previously described by others (Ref. 16).

Conclusions

The effects of shot peening low-stress ground surfaces on subsequent recrystallization tendencies in a single crystal superalloy were assessed. Specimens were prepared with shot peening at varied intensity and coverage, then given exposures at varied temperatures and times. The effects of these conditions on surface roughness and recrystallization were evaluated. Several conclusions could be drawn from this evaluation.

1. Shot peening using the current conditions on this single crystal superalloy can give roughness very similar to that produced in conventional polycrystalline superalloys, with minimized roughness produced by low intensities near 4 N and high coverage near 800 percent.

2. Recrystallization can be minimized by using low intensity shot peening near 4 N and low coverage near 100 percent, combined with exposures at relatively low temperatures and times near 1,200 °C (2,192 °F) and 1 h.
3. Alternatively, a consistent layer of recrystallized fine grains could be attained by using shot peening conditions at relatively high intensities combined with exposures at relatively high temperatures and short times.
4. For each of these alternative goals, the variability of recrystallization responses would need to be evaluated over greater lengths and multiple trials.
5. The limiting mechanical properties of intended applications would have to be closely considered for screening and selecting these conditions, as recrystallized grains could be detrimental to some properties.

References

1. Leverant, Gerald R.; and Kear, Bernard H.: The Mechanism of Creep in Gamma Prime Precipitation-Hardened Nickel-Base Alloys at Intermediate Temperatures. Metall. Trans., vol. 1, 1970, pp. 491–498.
2. VerSnyder, Francis L.; and Shank, M.E.: The Development of Columnar Grain and Single Crystal High Temperature Materials Through Directional Solidification. Mater. Sci. Eng., vol. 6, no. 4, 1970, pp. 213–247.
3. Fullagar, Keith P.L.; Broomfield, Robert W.; Hulands, Mark; Harris, Ken; Erickson, Gary L.; and Sikkenga, Steven L.: Aero Engine Test Experience With CMSX-4 Alloy Single Crystal Turbine Blades. ASME 94–GT–169, 1994.
4. Porter, A.; and Ralph, B.: The Recrystallization of Nickel-Base Superalloys. J. Mater. Sci., vol. 16, 1981, pp. 707–713.
5. Bond, S.D.; and Martin, J.W.: Surface Recrystallization in a Single Crystal Nickel-Based Superalloy. J. Mater. Sci., vol. 19, 1984, pp. 3867–3872.
6. Burgel, R.; Portella, P.D.; and Preuhs, J.: Recrystallization in Single Crystals of Nickel Base Superalloys. Proceedings of Ninth International Symposium on Superalloys, T.M. Pollock, R.D. Kissinger, R.R. Bowman, K.A. Green, M. McLean, S. Olson, and J.J. Schirra, eds., The Minerals, Metals & Materials Society, Warrendale, PA, 2000, pp. 229–238.
7. Cox, D.C.; Roebuck, B.; Rae, C.M.F.; and Reed, R.C.: Recrystallisation of Single Crystal Superalloy CMSX–4. Mater. Sci. Technol., vol. 19, 2003, pp. 440–446.
8. Zambaldi, C.; Roters, F.; Raabe, D.; and Glatzel, U.: Modeling and Experiments on the Indentation Deformation and Recrystallization of a Single-Crystal Nickel-Base Superalloy. Mater. Sci. Eng. A, vols. 454–455, 2007, pp. 433–440.
9. Panwisawas, Chinnapat; Mathur, Harshal; Gebelin, Jean-Christophe; Putman, Duncan; Rae, Catherine M.F.; and Reed, Roger C.: Prediction of Recrystallization in Investment Cast Single-Crystal Superalloys. Acta Mater., vol. 61, no. 1, 2013, pp. 51–66.
10. Harris, Ken; and Wahl, Jacqueline B.: Improved Single Crystal Superalloys, CMSX-4® (SLS)[La+Y] and CMSX-486®. Proceedings of the 10th International Symposium on Superalloys, K.A. Green, T.M. Pollock, H. Harada, T.E. Howson, R.C. Reed, J.J. Schirra, and S. Walston, eds., The Minerals, Metals, & Materials Society, Warrendale, PA, 2004, pp. 45–52.
11. Nguyen-Dinh, Xuan: Phase-Stable Single Crystal Materials. U.S. Patent 4,935,072, June 1990.
12. Dierksmeier, Douglas D.; and Heffernan, Tab M.: High Temperature Rotor Blade Attachment. U.S. Patent 5,688,108A, U.S. Patent Office, Nov. 1997.

13. Nesbitt, James A.; Miller, Robert A.; Gabb, Timothy P.; Draper, Susan L.; Locci, Ivan E.; and Sudbrack, Chantal K.: LCF Life of NiCr-Y Coated Disk Alloy After Shot Peening, Oxidation, and Hot Corrosion. NASA/TM—2020-220467, 2020. https://ntrs.nasa.gov
14. Jimenez, Pilar Gomez; Fish, Andrew; and Bosch, Cristina Estruch: Unlocking Scientific Knowledge With Statistical Tools in JMP®: Benefits and Challenges of New Statistical Tools. Johnson Matthey Technol. Rev., vol. 66, no. 2, 2022, pp. 198–211.
15. Nathal, M.V.; Bierer, J.; Evans, L.; Pogue, E.A.; Ritzert, F.; and Gabb, T.P.: Stress Relaxation Behavior in Single Crystal Superalloys. Mat. Sci. Eng. A, vol. 640, 2015, pp. 295–304.
16. Wang, Xin; Ma, Shicheng; Hu, Dianyin; Xu, Chunling; Luo, Xuekun; and Tang, Zhihui: Effect of Aging Temperature on the Fatigue Properties of Shot-Peened Single Crystal Superalloy at Intermediate Temperature. Int. J. Fatigue, vol. 156, no. 106675, 2022.
17. Wang, Xin; Xu, Chunling; Hu, Dianyin; Li, Chunzhi; Liu, Chenguang; and Tang, Zhihui: Effect of Ultrasonic Shot Peening on Surface Integrity and Fatigue Performance of Single-Crystal Superalloy. J. Mater. Process. Technol., vol. 296, no. 117209, 2021.
18. Xin, Wang; Zhihui, Tang; Chenguang, Liu; ChunZhi, Li; and Zhenye, Zhao: A Study on Single-Crystal Alloy Surface's Structure and Performance of Laser Shock Peening Without Absorbent Coating. AIP Conf. Proc., vol. 1783, no. 1, 2016.

TABLE I.—COMPOSITION IN WEIGHT PERCENT OF TESTED
SINGLE CRYSTAL SUPERALLOY COMPARED TO CMSX-4

Alloy, wt.%	Al	B	C	Co	Cr	Hf	Mo	Ni	Re	Si	Ta	Ti	W	Y	Zr	Note
Tested superalloy	5.04	--	0.003	10.02	5.40	0.09	1.75	Bal.	3.07	0.04	8.73	0.99	5.00	--	0.006	-------
CMSX-4	5.60	--	-----	9.00	6.50	0.10	0.60	Bal.	3.00	------	6.50	1.00	6.00	--	-----	Ref. 7

TABLE II.—CONDITIONS VARIED DURING
SHOT PEENING WITH CCW14 STEEL SHOT

Intensity, N	Coverage, percent			
	100	300	500	800
4	X	---	---	X
14	---	X	X	---
24	X	---	---	X

TABLE III.—SURFACE ROUGHNESS OF SINGLE CRYSTALS FOR VARIOUS SHOT PEENED SURFACES

Shot peening		Surface roughness					
Intensity, N	Coverage, percent	R_a mean, µm	R_a standard deviation, µm	R_{ms} mean, µm	R_{ms} standard deviation, µm	R_z mean, µm	R_z standard deviation, µm
4	100	0.66	0.02	0.84	0.03	5.17	0.43
4	800	0.60	0.10	0.77	0.08	4.51	0.63
14	300	1.39	0.18	1.74	0.22	9.50	1.21
14	500	1.42	0.18	1.80	0.23	9.72	1.00
24	100	2.48	0.30	3.14	0.24	17.26	2.18
24	800	1.90	0.43	2.38	0.47	12.72	2.03

TABLE IV.—DEPTH OF RECRYSTALLIZATION AND GRAIN SIZE
FOR VARIED SHOT PEENING AND EXPOSURES

Shot peening		Exposures		Recrystallization			
Intensity, N	Coverage, percent	Temperature, °C	Time, h	Depth of 50 percent recrystallization, µm	Depth mean, µm	Depth standard deviation, µm	Mean linear intercept grain size, µm
4	100	1,200	1	0.00	0.00	0.00	0.00
4	800	1,200	1	0.00	3.00	3.33	2.79
14	300	1,200	1	22.00	21.78	6.44	6.02
14	500	1,200	1	20.70	18.66	5.75	5.43
24	100	1,200	1	18.90	19.32	8.63	7.58
24	800	1,200	1	36.00	33.93	7.05	9.74
4	100	1,200	10	36.00	36.80	4.06	4.20
4	800	1,200	10	8.00	7.47	5.10	5.36
14	300	1,200	10	16.00	17.47	6.65	8.32
14	500	1,200	10	20.00	20.80	5.28	6.91
24	100	1,200	10	12.00	12.13	7.27	8.69
24	800	1,200	10	36.80	40.57	7.62	7.36
4	100	1,300	1	2.40	5.76	7.61	10.58
4	800	1,300	1	8.00	18.93	19.53	5.91
14	300	1,300	1	36.80	37.65	20.89	9.13
14	500	1,300	1	25.60	34.13	18.91	8.34
24	100	1,300	1	25.60	31.89	15.92	5.77
24	800	1,300	1	38.40	44.80	20.52	8.09
4	100	1,300	10	10.50	9.45	4.48	8.40
4	800	1,300	10	14.40	13.36	3.60	7.80
14	300	1,300	10	96.30	100.44	18.47	40.00
14	500	1,300	10	67.50	66.10	9.99	26.00
24	100	1,300	10	209.70	206.64	15.93	88.95
24	800	1,300	10	185.40	188.70	15.27	49.03

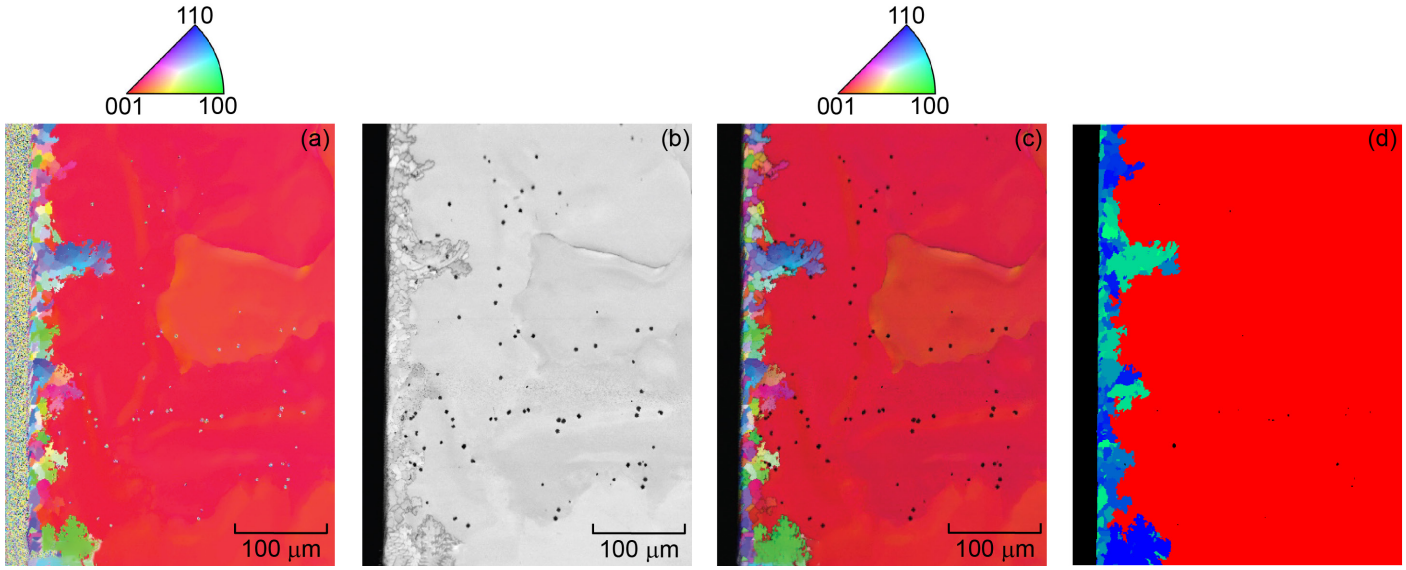

Figure 1.—Shot peened specimens. (a) Raw inverse pole figure (IPF-Z) map. (b) Image quality (IQ) map. (c) Overlaid IPF-Z–IQ map. (d) Processed unique grain map.

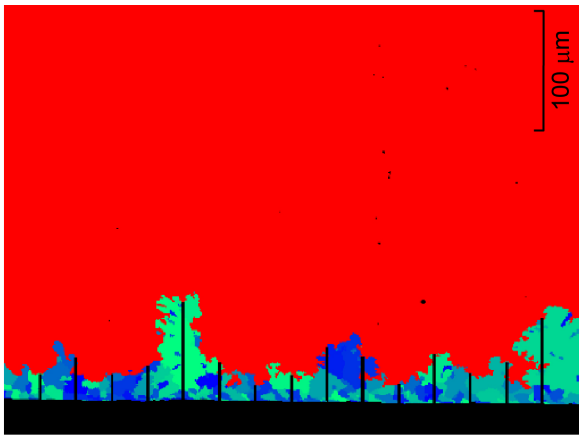

Figure 2.—Recrystallization depths measured at 15 evenly spaced locations along length of image.

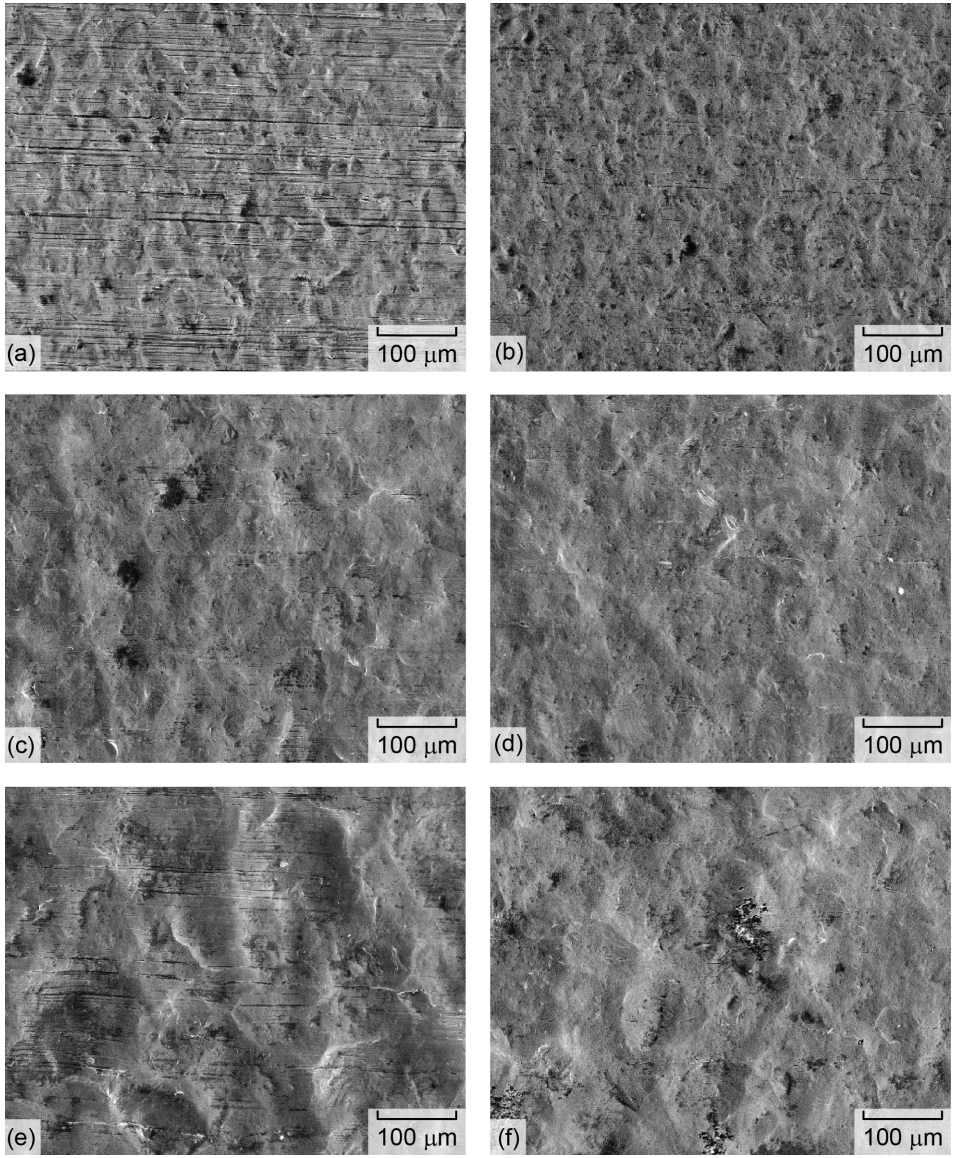

Figure 3.—Shot peened surfaces of single crystals before exposures at varied intensities and percent coverage. (a) 4 N, 100 percent. (b) 4 N, 800 percent. (c) 14 N, 300 percent. (d) 14 N, 500 percent (e) 24 N, 100 percent. (f) 24 N, 800 percent.

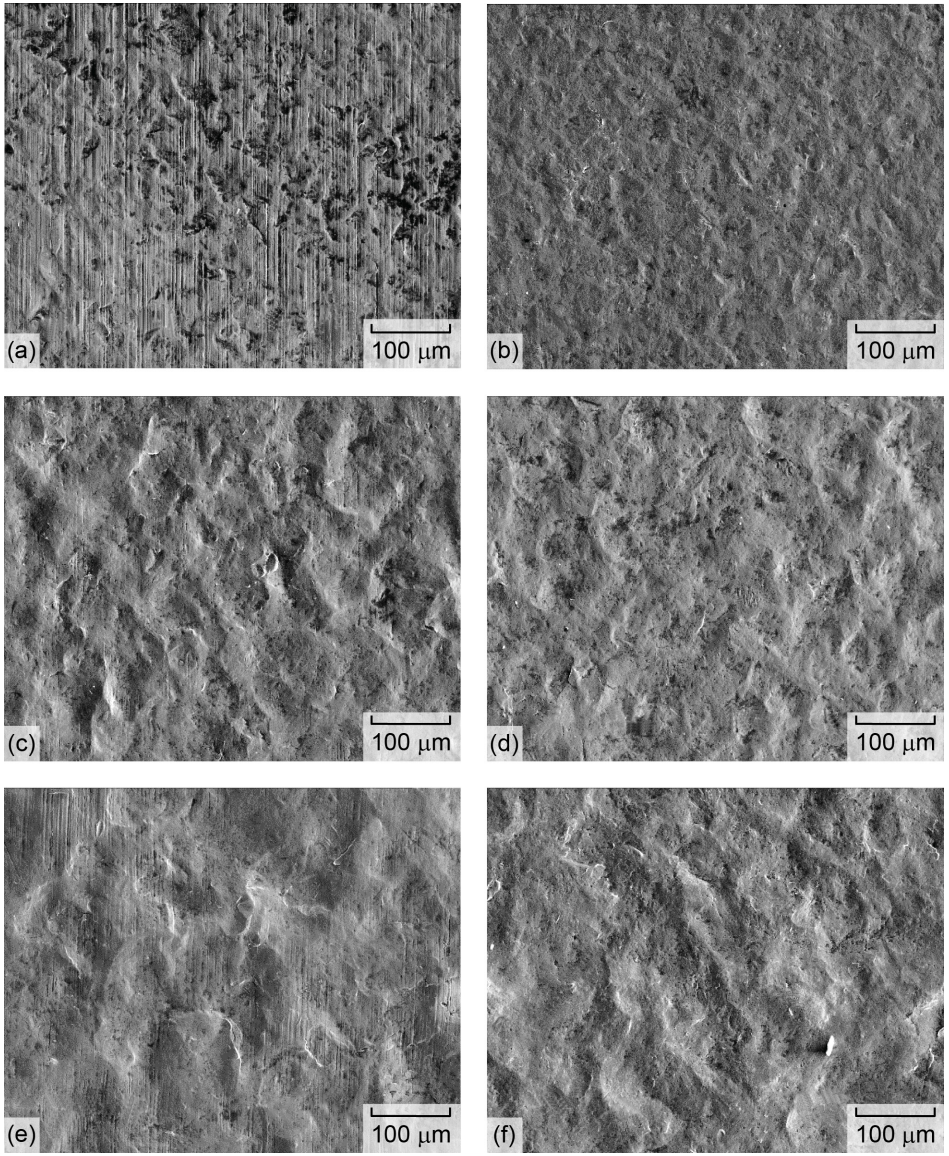

Figure 4.—Shot peened surfaces of LSHR witness specimens at varied intensities and percent coverage. (a) 4 N, 100 percent. (b) 4 N, 800 percent. (c) 14 N, 300 percent. (d) 14 N, 500 percent. (e) 24 N, 100 percent. (f) 24 N, 800 percent.

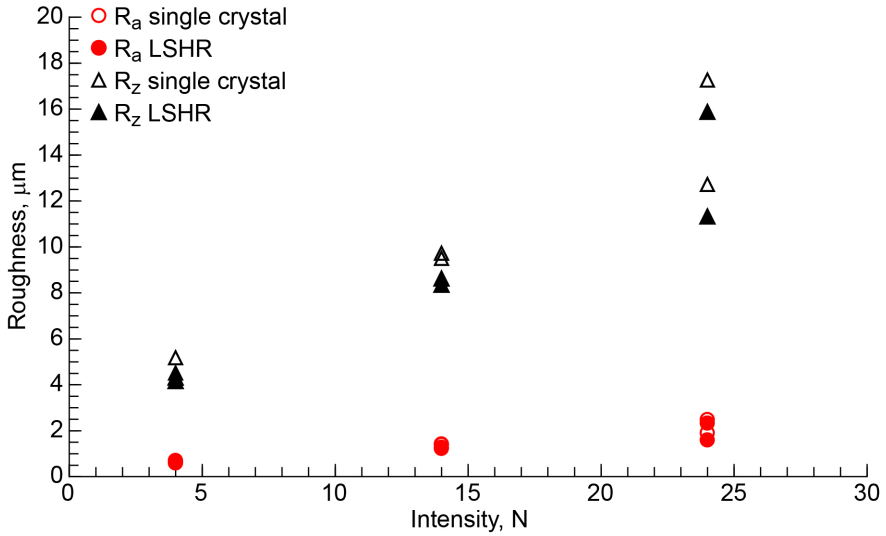

Figure 5.—Average roughness (R_a) and peak-valley roughness (R_z) of single crystal test specimens and LSHR witness specimens versus shot peening intensity.

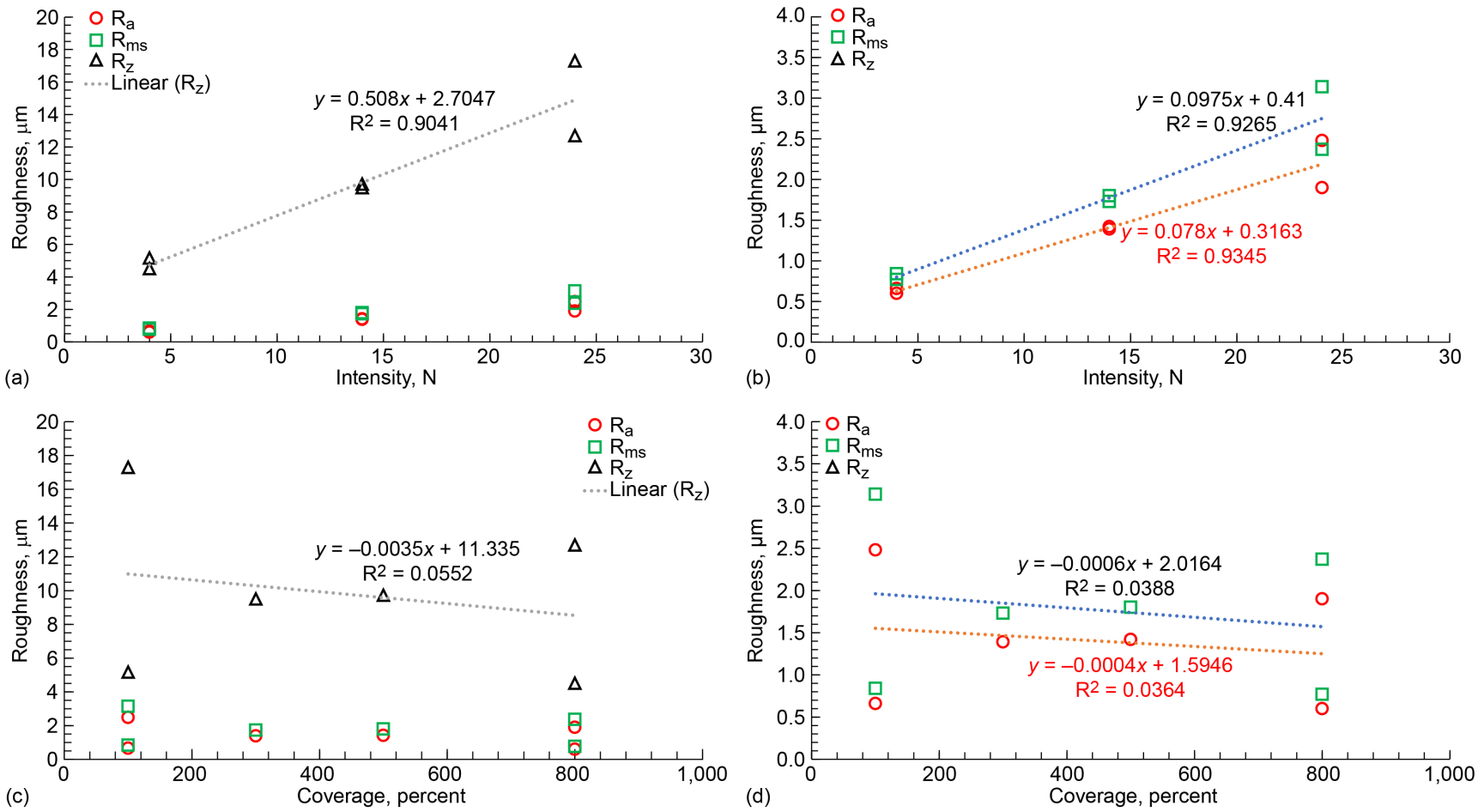

Figure 6.—Roughness of single crystals. (a) Versus shot peening intensity. (b) Versus shot peening intensity with y-axis varied for resolution. (c) Versus shot peening coverage. (d) Versus shot peening coverage with y-axis varied for resolution.

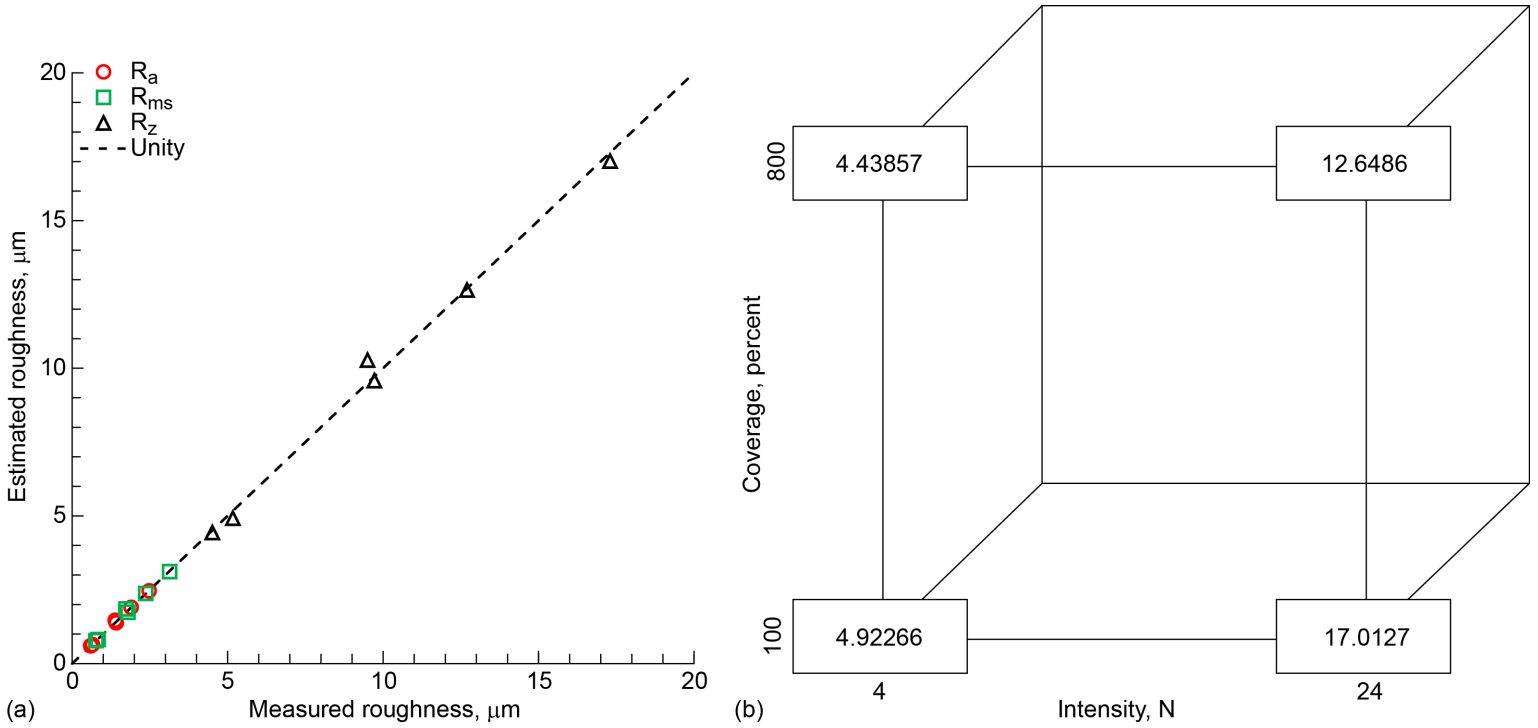

Figure 7.—Single crystal roughness. (a) Measured versus linear regression estimated average roughness (R_a), root mean square roughness (R_{ms}), and peak-valley roughness (R_z). (b) Estimated mean values in microns of peak-valley roughness (R_z) with increasing intensity and coverage.

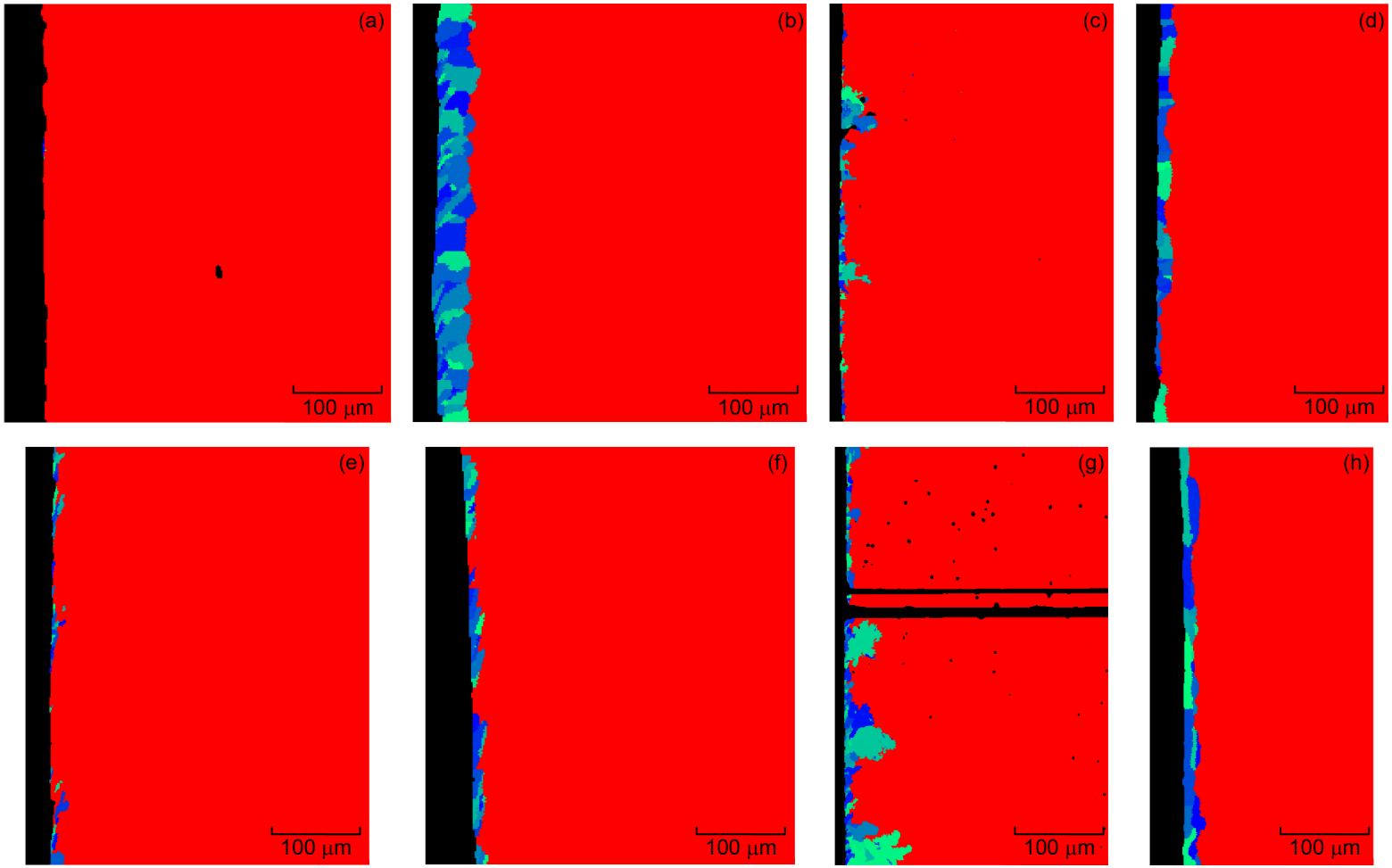

Figure 8.—Typical EBSD images of single crystal cross sections subjected to shot peening plus high-temperature exposures. (a) 4 N, 100 percent, exposed at 1,200 °C for 1 h. (b) 4 N, 100 percent, exposed at 1,200 °C for 10 h. (c) 4 N, 100 percent, exposed at 1,300 °C for 1 h. (d) 4 N, 100 percent, exposed at 1,300 °C for 10 h. (e) 4 N, 800 percent, exposed at 1,200 °C for 1 h.(f) 4 N, 800 percent, exposed at 1,200 °C for 10 h, (g) 4 N, 800 percent, exposed at 1,300 °C for 1 h. (h) 4 N, 800 percent, exposed at 1,300 °C for 10 h.

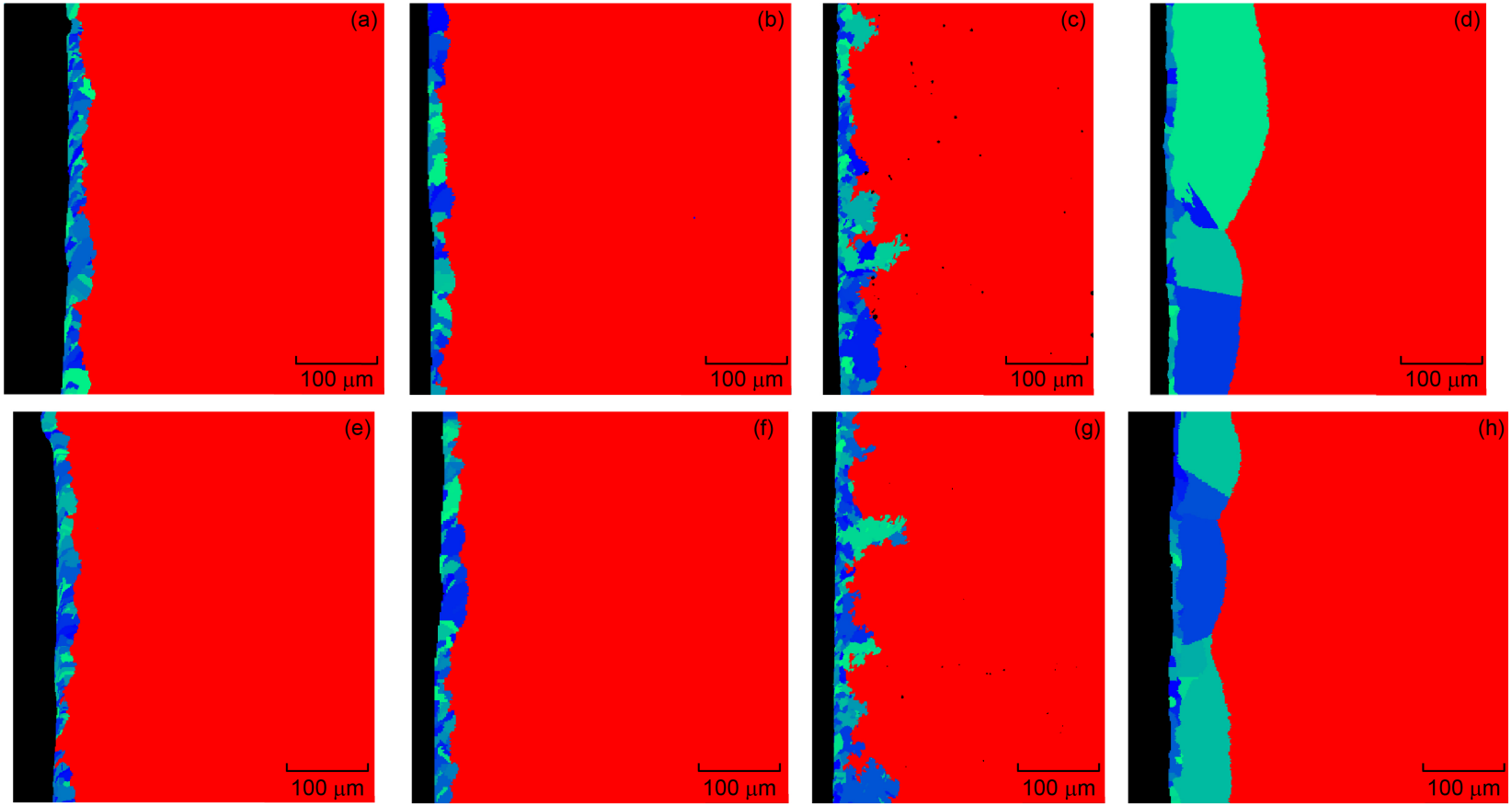

Figure 9.—Typical EBSD images of single crystal cross sections subjected to shot peening plus high-temperature exposures. (a) 14 N, 300 percent, exposed at 1,200 °C for 1 h. (b) 14 N, 300 percent, exposed at 1,200 °C for 10 h. (c) 14 N, 300 percent, exposed at 1,300 °C for 1 h. (d) 14 N, 300 percent, exposed at 1,300 °C for 10 h. (e) 14 N, 500 percent, exposed at 1,200 °C for 1 h. (f) 14 N, 500 percent, exposed at 1,200 °C for 10 h. (g) 14 N, 500 percent, exposed at 1,300 °C for 1 h. (h) 14 N, 500 percent, exposed at 1,300 °C for 10 h.

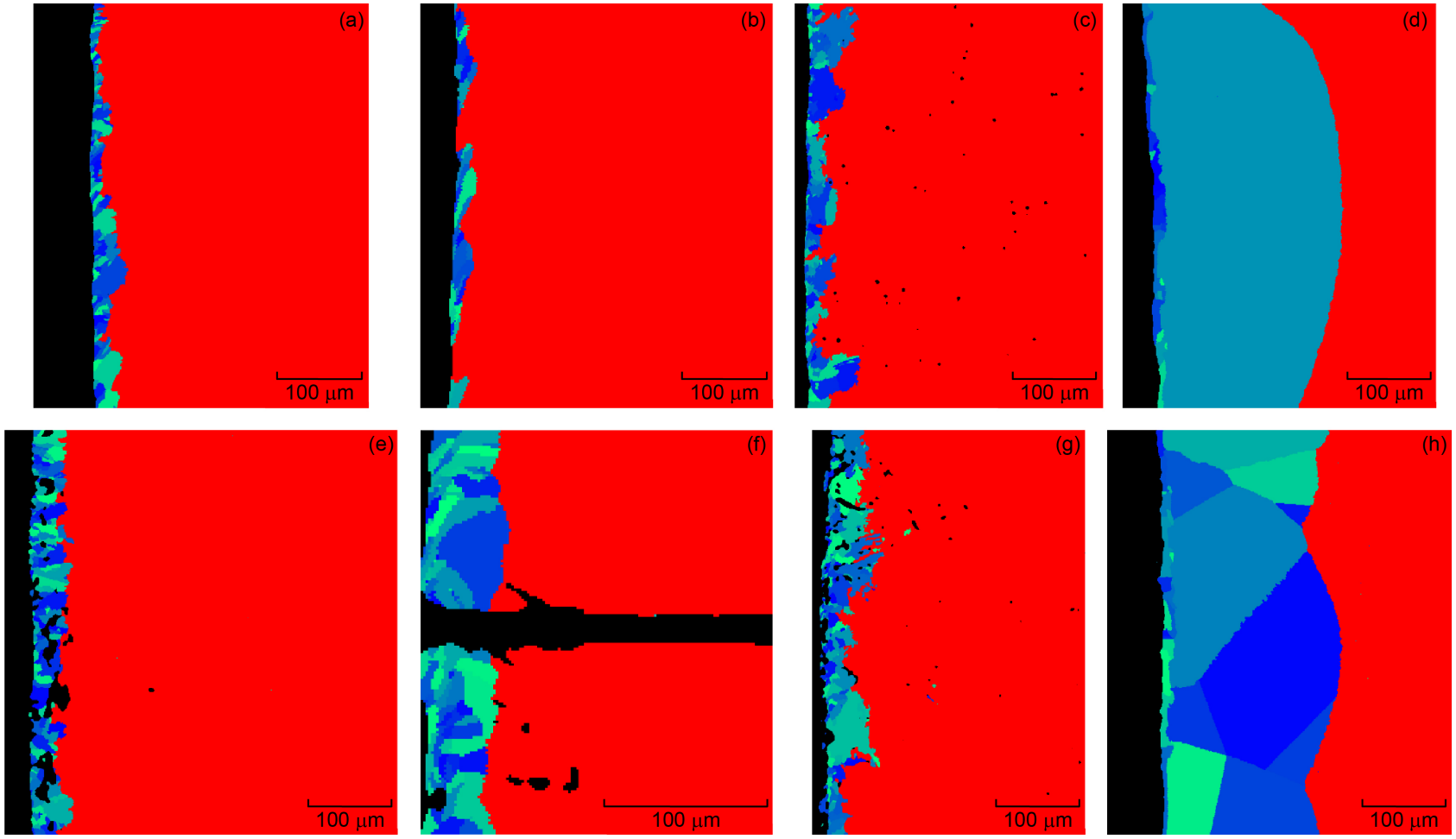

Figure 10.—Typical EBSD images of single crystal cross sections subjected to shot peening plus high-temperature exposures. (a) 24 N, 100 percent, exposed at 1,200 °C for 1 h. (b) 24 N, 100 percent, exposed at 1,200 °C for 10 h. (c) 24 N, 100 percent, exposed at 1,300 °C for 1 h. (d) 24 N, 100 percent, exposed at 1,300 °C for 10 h. (e) 24 N, 800 percent, exposed at 1,200 °C for 1 h. (f) 24 N, 800 percent, exposed at 1,200 °C for 10 h. (g) 24 N, 800 percent, exposed at 1,300 °C for 1 h. (h) 24 N, 800 percent, exposed at 1,300 °C for 10 h.

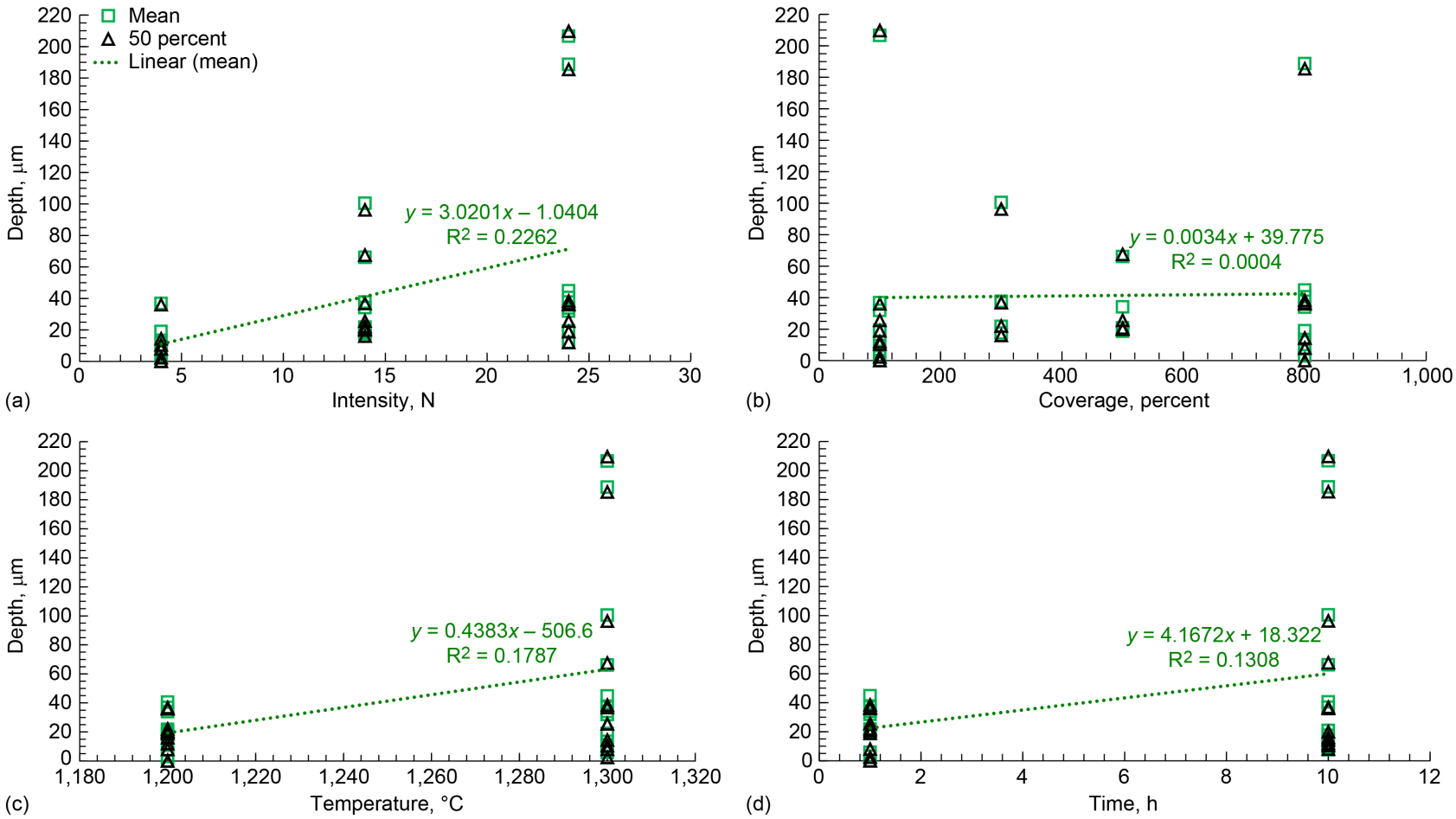

Figure 11.—Mean depth of recrystallization and 50 percent recrystallized depths. Linear regression equation and coefficient of determination (R^2) are indicated for mean depth. (a) Versus shot peening intensity. (b) Versus shot peening coverage. (c) Versus exposure temperature (d) Versus exposure time.

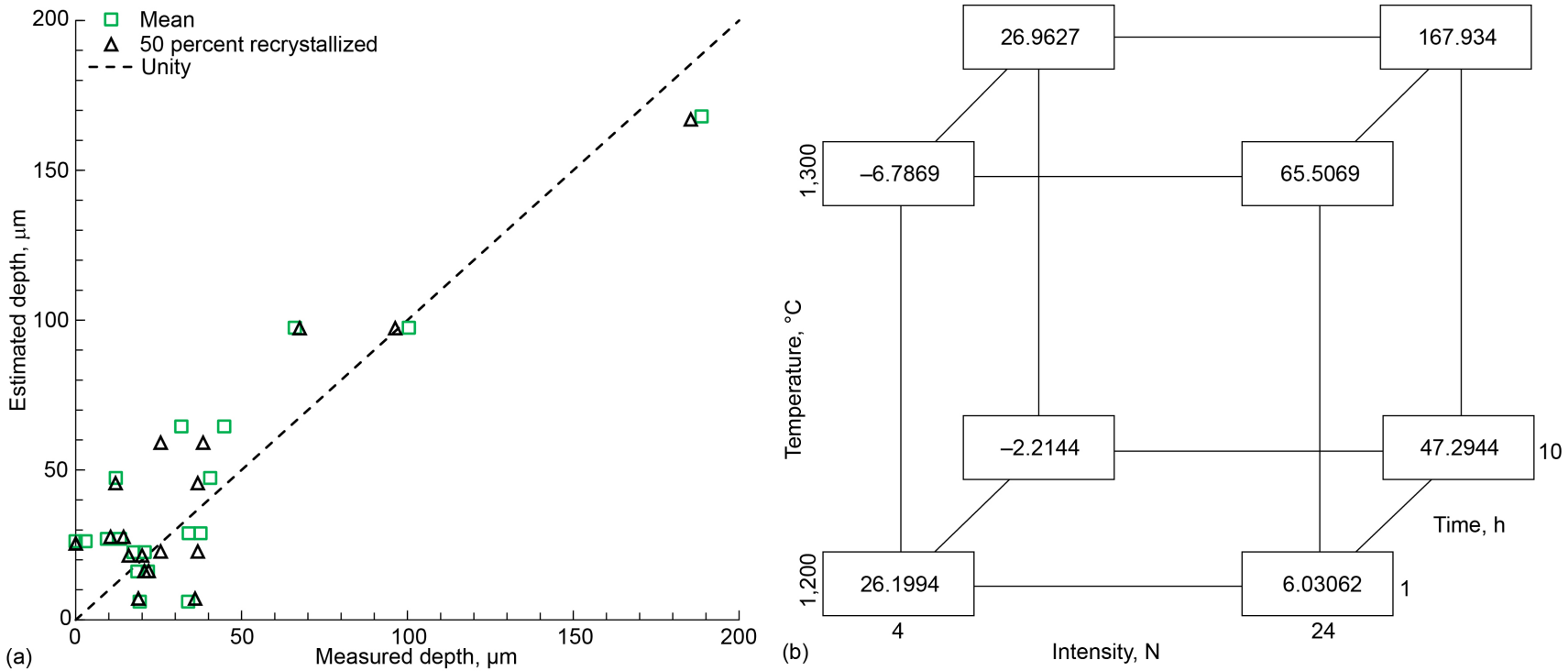

Figure 12.—Single crystal recrystallization depth. (a) Linear regression estimated versus measured depths of recrystallization. (b) Estimated values of mean depth in microns with increasing shot peening intensity, exposure temperature, and exposure time.

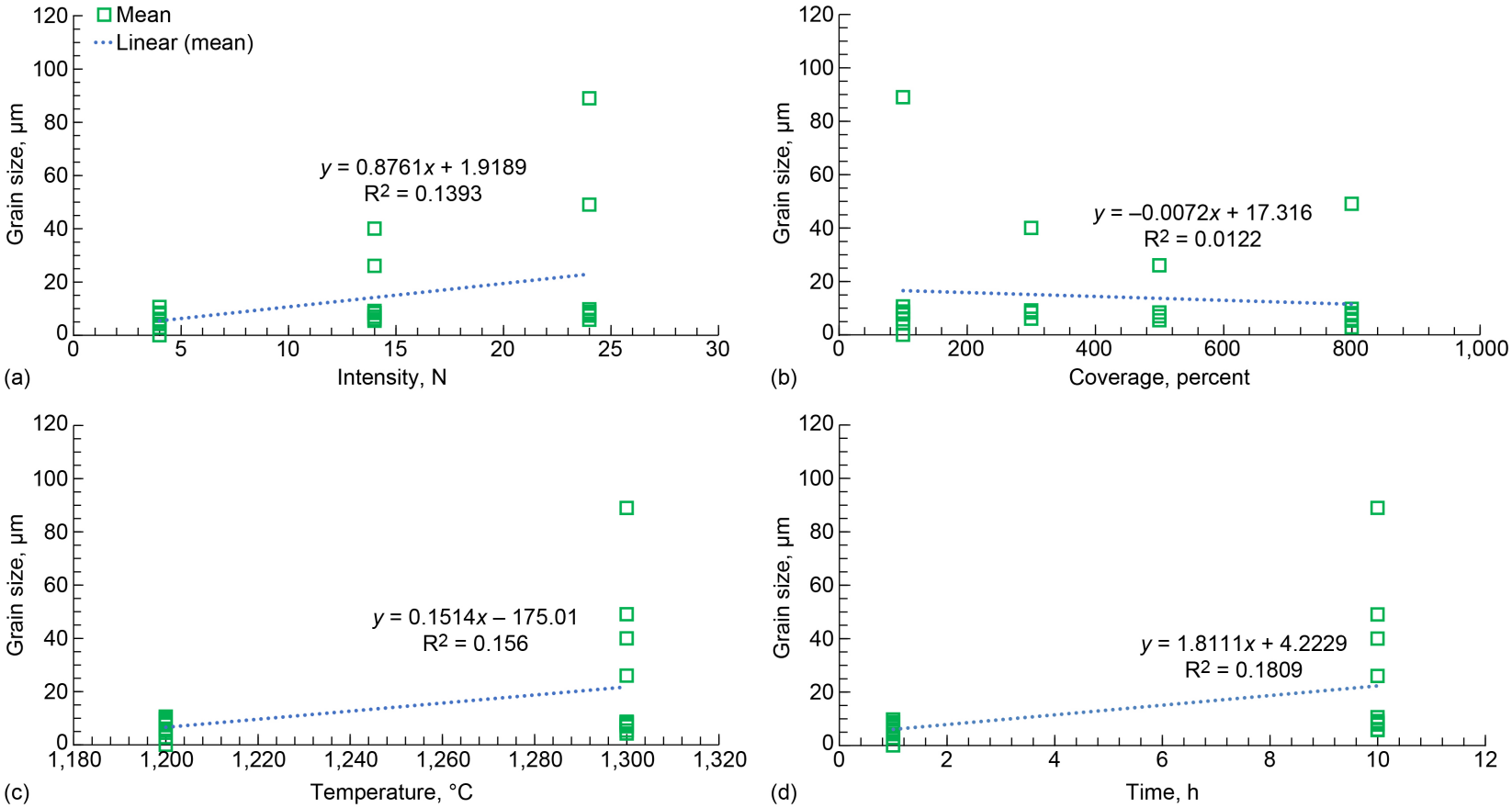

Figure 13.—Mean linear intercept grain size measured perpendicular to surface. Linear regression equation and coefficient of determination (R^2) are indicated. (a) Versus shot peening intensity. (b) Versus shot peening coverage. (c) Versus exposure temperature. (d) Versus exposure time.

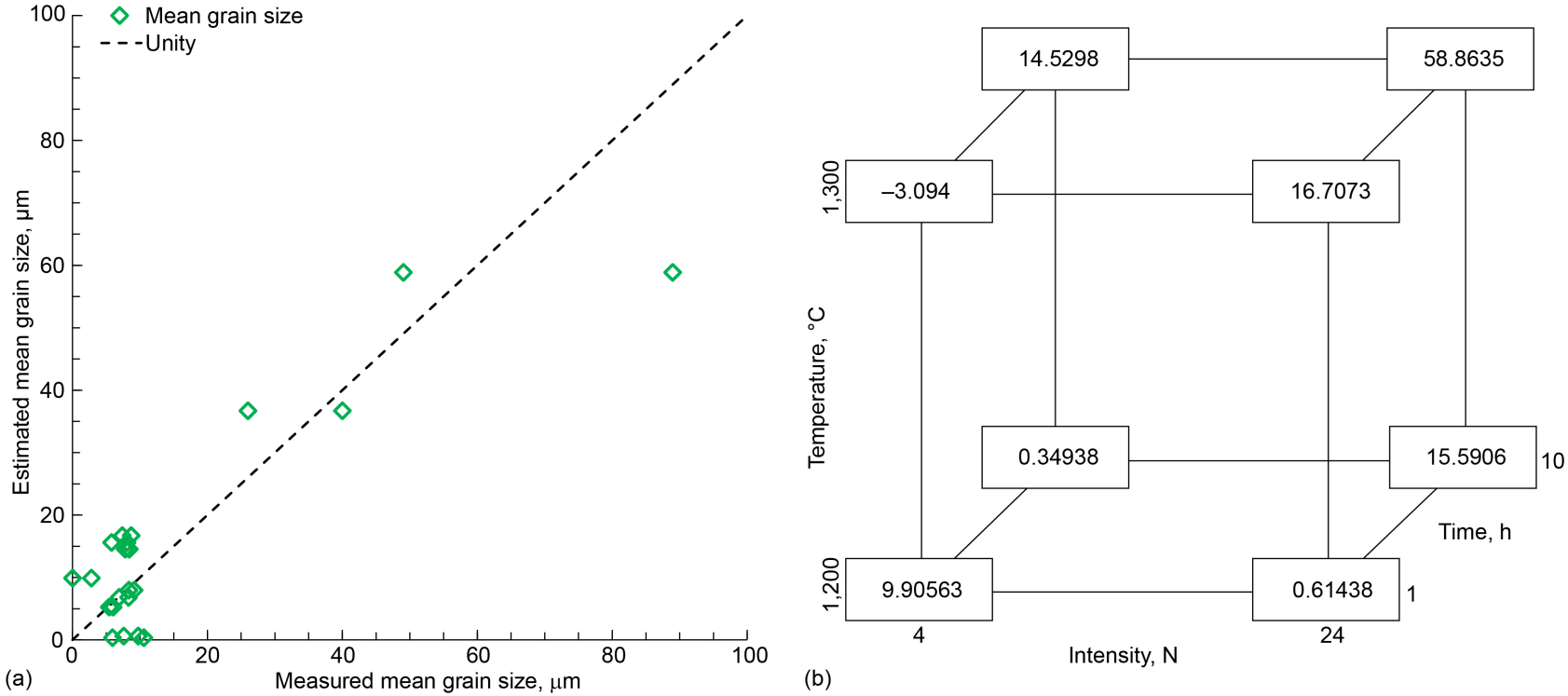

Figure 14.—Recrystallized grain widths. (a) Linear regression estimated versus measured mean linear intercept widths of recrystallized grains. (b) Estimated values of mean grain size in microns with increasing shot peening intensity, exposure temperature, and exposure time.